Available online at www.sciencedirect.com
ScienceDirect
International Journal of Heat and Mass Transfer 50 (2007) 4883–4890
International Journal of HEAT and MASS TRANSFER
www.elsevier.com/locate/ijhmt

Influence of pulsatile blood flow and heating scheme on the temperature distribution during hyperthermia treatment

Khalil Khanafer [a], Joseph L. Bull [a], Ioan Pop [b,*], Ramon Berguer [a,c]

[a] Vascular Mechanics Lab, Biomedical Engineering Department, University of Michigan, Ann Arbor, MI 48109, USA
[b] Faculty of Mathematics, University of Cluj, R-3400 Cluj, Romania
[c] Vascular Mechanics Lab, Section of Vascular Surgery, University of Michigan, Ann Arbor, MI 48109, USA

Received 15 January 2007
Available online 15 May 2007

Abstract

We conducted a numerical study to determine the influence of pulsatile laminar flow and heating protocol on temperature distribution in a single blood vessel and tumor tissue receiving hyperthermia treatment. We utilized both a physiological resting waveform at time-averaged Reynolds number of 50 and 300 and a sinusoidal waveform in this investigation. The arterial wall was modeled using the volume-averaged porous media equations. Discretization of the transport equations was achieved using a finite element scheme based on the Galerkin method of weighted residuals. We validated our numerical model by comparing it with previously published results in literature. Our results indicate that the choice of waveform significantly influences the findings concerning temperature distribution and heat transfer rate during hyperthermia treatment. A comprehensive analysis of the influence of blood velocity pulsations and blood vessel size on temperature uniformity of tissues undergoing hyperthermia treatment is presented in detail. The results of the present investigation illustrate that large vessels have a profound effect on the heat transfer characteristics in tissues receiving hyperthermia treatment. The results of this work may enhance current understanding of the factors that determine the effect of hyperthermia treatment on tumor tissues.

Keywords: Pulsatile flow; Hyperthermia; Galerkin numerical solution

1. Introduction

Hyperthermia treatment has been demonstrated as effective during cancer therapy in recent years. Its objective is to raise the temperature of pathological tissues above cytotoxic temperatures (41–45 °C) without overexposing healthy tissues [1–4]. Although difficult to achieve and maintain in a clinical setting, uniform temperature distributions, are significant during hyperthermia treatment [5] since the use of temperatures above 55 °C may directly destroy tissues through thermal coagulation, as was illustrated by Beacco et al. [6]. Temperature variations, which may be associated with the mechanisms of heat removal by the body and may sometimes be caused by inadequate heating technologies, are often heterogeneous, and can lead to defectively heated tissues, hot spots and potential burning.

Temperature distribution within tissues primarily depends on tissue thermal conductivity, the heating source's power deposition pattern characteristics, and heat transfer resulting from blood flow [7]. An important source of temperature non-uniformity is the presence of large vessels entering the heated volume and carrying blood at a lower systemic temperature (37 °C). Blood flow has a profound influence on the efficiency of thermal therapy treatment. The design of delivered power devices and numerous theoretical, experimental, and clinical studies have demonstrated that large blood vessels may produce localized cooling regions within heated tissues during

* Corresponding author. Tel.: +40 264 594 315; fax: +40 264 591 906.
E-mail address: pop.ioan@yahoo.co.uk (I. Pop).

0017-9310/$ - see front matter © 2007 Elsevier Ltd. All rights reserved.
doi:10.1016/j.ijheatmasstransfer.2007.01.062

Nomenclature

d	blood vessel diameter
K	permeability
L	blood vessel length
p	blood pressure
r	radial distance
$\mathbf{R}_1$, $\mathbf{R}_2$, and $\mathbf{R}_3$	residuals (errors)
Re_m	time-averaged Reynolds number ($=d\bar{u}_m/\upsilon$)
T	temperature
u_r	radial velocity
u_z	axial velocity
$\bar{u}_m$	time-averaged inlet mean velocity
$\mathbf{v}$	velocity vector
z	longitudinal coordinate

Greek symbols

α	thermal diffusivity of blood
ρ	blood density
μ	fluid dynamic viscosity
φ	interpolation function for velocity
ε	porosity
ψ	interpolation function for pressure
ϑ	interpolation function for temperature
τ	time
ν	fluid kinematic viscosity ($=\mu/\rho$)

Subscripts

f	fluid
e	effective properties

Other

$\langle\rangle$	the local volume average of a quantity

hyperthermia treatment [8–11]. Kolios et al. [12] investigated the effect of large blood vessel in heated tissues and showed that the dissipation of heat from heated tissues was carried out by convection through blood flow and also by conduction process. In another study, Kolios et al. [13] demonstrated that blood flow through large blood vessels plays an important role in determining temperature profiles of heated tissues even when the treatment time is within 3–20 s. Furthermore, Crezee and Lagendijk [5] conducted a numerical study on the impact of large vessels on the temperature uniformity during hyperthermia treatment assuming steady-state condition; this study revealed that the presence of a large vessel may result in non-uniform temperature resulting in possible under dosage. All of the aforementioned studies focused on determining temporal variations of temperature in tissue while assuming a steady-state blood flow whereas, in the human use of hyperthermia, blood flow is periodically oscillating.

Several studies have also been conducted to analyze the effect of oscillatory flow on the velocity profile without examining its effect on heat transfer [14–17]. However, later studies, like the early work by Siegel and Perlmutter [18], addressed the dependence of heat transfer characteristics on pulsatile flow in a channel. Cho and Hyun [19] assumed a sinusoidal variation of the velocity at the pipe inlet in a numerical study of pulsatile flow and heat transfer characteristics within a pipe. Kim et al. [20] analyzed numerically the heat transfer characteristics of fully developed pulsatile flow in a channel, assuming a sinusoidal variation of the velocity at the inlet of the channel. The limitation of these studies was that they considered dimensions and parameters that are not applicable to human vasculature.

Recently, Shih et al. [21] investigated the cooling effects of thermally significant blood vessels in perfused tissue during thermal therapy using Pennes bioheat transfer equation. Their results showed that the cooling effect of blood vessels was more obvious for longer heating. Craciunescu and Clegg [22] studied numerically the effect of blood velocity pulsations on temperature distribution and heat transfer within rigid blood vessels and assumed the entrance velocity to be a simple sinusoidal function of time. The authors assumed a sinusoidal velocity waveform at the inlet of the blood vessel and neglected the effect of arterial wall on the blood temperature distribution and wall temperature variation. Also, they only focused on the heat transfer between blood flow and vessel wall, not considering heat exchange between the tissue and blood vessel in whole. Their results illustrated that pulsating axial velocity produces pulsating temperature variation and a reversal of flow within the aorta and large vessels.

Therefore, the purpose of the present study is to compare the physiological flow and heat transfer characteristics in a single blood vessel with those obtained under the assumption of a sinusoidal velocity waveform while considering the influence of blood vessel size and the arterial wall on temperature uniformity of tissues receiving hyperthermia treatment. We also investigated the impact of different heating protocols on the transient temperature distribution in both blood vessel and the arterial wall.

2. Mathematical formulation

Consider unsteady, axi-symmetric incompressible Newtonian blood flow through a rigid vessel of length L, thickness t, and radius R. The geometry of the problem and the coordinate system are shown in Fig. 1. The blood flow and temperature in the artery lumen is described by continuity, Navier–Stokes, and energy equations using cylindrical polar coordinates as follows:

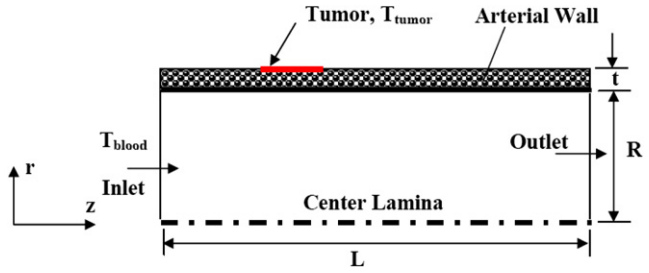

Fig. 1. Schematic of the physical and coordinate system.

$$\frac{1}{r}\frac{\partial}{\partial r}(ru_r)+\frac{\partial u_z}{\partial z}=0 \tag{1}$$

$$\frac{\partial u_z}{\partial \tau}+u_r\frac{\partial u_z}{\partial r}+u_z\frac{\partial u_z}{\partial z}=-\frac{1}{\rho}\frac{\partial p}{\partial z}+\nu\left(\frac{\partial^2 u_z}{\partial z^2}+\frac{\partial^2 u_z}{\partial r^2}+\frac{1}{r}\frac{\partial u_z}{\partial r}\right) \tag{2}$$

$$\frac{\partial u_r}{\partial \tau}+u_r\frac{\partial u_r}{\partial r}+u_z\frac{\partial u_r}{\partial z}=-\frac{1}{\rho}\frac{\partial p}{\partial r}+\nu\left(\frac{\partial^2 u_r}{\partial z^2}+\frac{\partial^2 u_r}{\partial r^2}+\frac{1}{r}\frac{\partial u_r}{\partial r}-\frac{u_r}{r^2}\right) \tag{3}$$

$$\frac{\partial T}{\partial \tau}+u_r\frac{\partial T}{\partial r}+u_z\frac{\partial T}{\partial z}=\alpha\left(\frac{1}{r}\frac{\partial}{\partial r}\left(r\frac{\partial T}{\partial r}\right)+\frac{\partial^2 T}{\partial z^2}\right) \tag{4}$$

where u_z and u_r are the axial and radial velocity, respectively, p the pressure, T the temperature, α the thermal diffusivity of blood, and ν is the kinematic viscosity of blood. The arterial wall is modeled as macroscopically homogeneous porous media [23,24]. Therefore, the volume-averaged governing equations are (Vafai and Tien [25,26], Alazmi and Vafai [27], Khanafer et al. [28], Nield [29], Ingham and Pop [30], Pop and Ingham [31]):

$$\nabla\cdot\langle\mathbf{v}\rangle=0 \tag{5}$$

$$\frac{\rho_f}{\varepsilon}\left[\frac{\partial\langle\mathbf{v}\rangle}{\partial\tau}+\langle(\mathbf{v}\cdot\nabla)\mathbf{v}\rangle\right]=-\nabla\langle p\rangle^f+\frac{\mu_f}{\varepsilon}\nabla^2\langle\mathbf{v}\rangle-\frac{\mu_f\langle\mathbf{v}\rangle}{K} \tag{6}$$

$$\frac{\partial T}{\partial \tau}+u_r\frac{\partial T}{\partial r}+u_z\frac{\partial T}{\partial z}=\alpha_e\left(\frac{1}{r}\left(r\frac{\partial T}{\partial r}\right)+\frac{\partial^2 T}{\partial z^2}\right) \tag{7}$$

where $\langle\rangle$ denotes the local volume average of a quantity (Vafai and Tien [25,26]), $\mathbf{v}$ the velocity vector, f the superscript that refers to the local volume average inside the fluid, K the permeability, α_e the effective thermal diffusivity, and ε is the porosity. The effective thermal properties are related to fluid and solid matrix properties by the following relations:

$$(\rho c_p)_e=\varepsilon(\rho c_p)_f+(1-\varepsilon)(\rho c_p)_s \tag{8}$$

$$k_e=\varepsilon k_f+(1-\varepsilon)k_s \tag{9}$$

where the subscript s refers to solid matrix properties (i.e. arterial wall) and f refers to blood properties. Eqs. (1)–(7) require suitable boundary conditions. The following boundary conditions are applied: fully developed pulsating velocity at the inlet to the arterial lumen is specified as:

$$u_z(r,t)=2\bar{u}_m(t)\left[1-\left(\frac{r}{R}\right)^2\right] \tag{10}$$

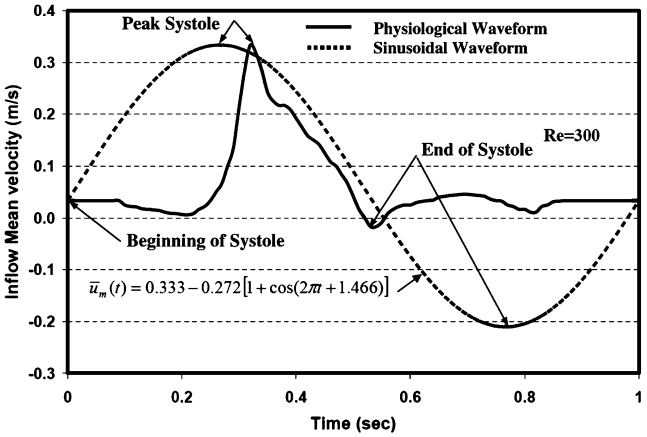

Fig. 2. Time variation of the inflow mean velocity for physiological and sinusoidal pulsatile flows.

The time-averaged Reynolds number is defined as:

$$Re_m=\frac{\rho\bar{u}_m d}{\mu_f} \tag{11}$$

where $\bar{u}_m$ is the time-averaged inlet mean velocity (Fig. 2) and μ_f is the viscosity of the blood. A waveform corresponding to a resting person was used for the time dependent inlet mean velocity, $\bar{u}_m(t)$, as reported by Mills et al. [32] to approximate *in vivo* measurements as shown in Fig. 2. This pulse was generally considered for $Re_m\approx 300$ as illustrated by Pedersen et al. [33,34]. Zero transverse velocity gradient and zero cross-flow on the axis of symmetry $\left(r=0:v=\frac{\partial u}{\partial r}=0\right)$, a traction-free condition at the outlet in the lumen and wall, and zero transverse velocity at the inlet region of the wall. For this study, we assumed that a single large artery was embedded within the tissue in order to determine the effects of blood flow with physiological waveforms on the temperature distribution in the treated region. We view this as the first of many steps needed to model the more complex physiological situation. In the actual physiological situation, larger arteries are usually near a corresponding vein. These vessels have different diameters

Table 1
Physiological parameters used in the numerical simulation [35]

Layer	Parameters	Value
Lumen	Density, ρ (kg/m^3)	1050
	Dynamic viscosity, μ (kg/m s)	0.00345
	Conductivity, k (W/m K)	0.51
	Specific heat, c (kJ/kg K)	3.78
Endothelium	Permeability, K (m^2)	4.32×10^{-15}
	Porosity, ε	0.0005
Intima	Permeability, K (m^2)	2×10^{-10}
	Porosity, ε	0.983
IEL (internal elastic lamina)	Permeability, K (m^2)	4.39×10^{-13}
	Porosity, ε	0.002
Media	Permeability, K (m^2)	2×10^{-12}
	Porosity, ε	0.258

and flow rates, and their flows are countercurrent. The configuration of the vessels depends on the specific tissue. As such, the heat exchange between the two blood vessels should be considered in more complicated models. The goal of this first model is to demonstrate the effect of pulsatile flow in hyperthermia treatments. It is also assumed in this study that the influence of the heating technique (e.g. ultrasound, microwave, etc.) is described by setting a fixed temperature for the tumor which is higher than the inlet blood temperature (i.e. $T_{\text{tumor}} > T_{\text{blood}}$). Further, the absorption of the delivered energy to the surrounding tissue around the vessel is not considered. The physiological properties for various layers used in our model are based upon appropriate pore theory, fiber matrix models, and *in vivo* and *in vitro* experiments are tabulated in Table 1 [35].

3. Heat transfer calculations

The non-dimensional heat flux is expressed in this study as follows:

$$q = \frac{\partial \theta}{\partial n} \tag{12}$$

where n denotes the normal pointing outward from the surface over which the heat flux is to be calculated.

4. Numerical scheme

A finite element formulation based on the Galerkin method is employed to solve the governing equations subject to the boundary conditions for the present study. The objective of the finite element method is to reduce the system of governing equations into a discretized set of continuum problem algebraic equations. The finite element procedure begins with the division of the continuum region of interest into a number of simply shaped regions called elements. These elements are assumed to be fixed in the space. Within each element, the dependent variables velocity u_i, pressure p, and temperature T fields are approximated by the following equations:

$$u_i = \varphi^{\mathrm{T}} \mathbf{U}_i(t) \tag{13}$$

$$p = \psi^{\mathrm{T}} \mathbf{P}(t) \tag{14}$$

$$T = \vartheta^{\mathrm{T}} \mathbf{T}(t) \tag{15}$$

where $\mathbf{U}_i$, $\mathbf{P}$ and $\mathbf{T}$ are column vectors of element nodal point unknowns and φ, ψ, and ϑ are column vectors of the interpolation functions for velocity, pressure, and temperature, respectively. Substitution of these approximations into the field equations for continuity and yields a set of equations for the residual error as given below:

$$\text{Continuity:} \quad \mathbf{f}_1(\varphi, \mathbf{U}_i) = \mathbf{R}_1 \tag{16}$$

$$\text{Momentum:} \quad \mathbf{f}_2(\varphi, \psi, \vartheta, \mathbf{U}_i, \mathbf{P}, \mathbf{T}) = \mathbf{R}_2 \tag{17}$$

$$\text{Energy:} \quad \mathbf{f}_3(\varphi, \theta, \mathbf{U}_i, \mathbf{T}) = \mathbf{R}_3 \tag{18}$$

where $\mathbf{R}_1$, $\mathbf{R}_2$, and $\mathbf{R}_3$ are the residuals (errors) resulting from the use of the finite element approximations. The Galerkin form of the method of weighted residuals seeks to reduce these errors to zero, in a weighted sense, by making the residuals orthogonal to the interpolation functions of each element. These orthogonality conditions are given by:

$$(\mathbf{f}_1, \varphi) = (\mathbf{R}_1, \varphi) = 0 \tag{19}$$

$$(\mathbf{f}_2, \psi) = (\mathbf{R}_2, \psi) = 0 \tag{20}$$

$$(\mathbf{f}_3, \vartheta) = (\mathbf{R}_3, \vartheta) = 0 \tag{21}$$

The two-dimensional 9-node quadrilateral element was used in this study. The velocity and temperature are approximated using biquadratic interpolation functions. The highly coupled and non-linear algebraic equations resulting from the discretization of the governing equations are solved using the segregated solution algorithm. The advantage of using this method is that the global system matrix is decomposed into smaller submatrices and then solved in a sequential manner. The conjugate residual scheme is used to solve the symmetric pressure-type equation systems, while the conjugate gradient squared method is used for the non-symmetric advection–diffusion-type equations. A variable grid-size system is implemented in the present investigation to capture the rapid changes in the dependent variables. Extensive numerical runs are performed to attain grid-independent results. Solution for Stokes flow problem was utilized as an initial condition for solving the above equations until the flow became time periodic. Thus, regardless of the initial condition, a sufficient number of cycles were performed to overcome the transition period and achieve convergence for repetitive solutions at successive cycles. We considered the solution to be converged when the relative change in variables between consecutive iterations was less than 10^{-5}.

5. Model validation

The results of the present numerical scheme were validated against the experimental and analytical results of Atabek and Chang [16] for laminar, oscillatory flow in

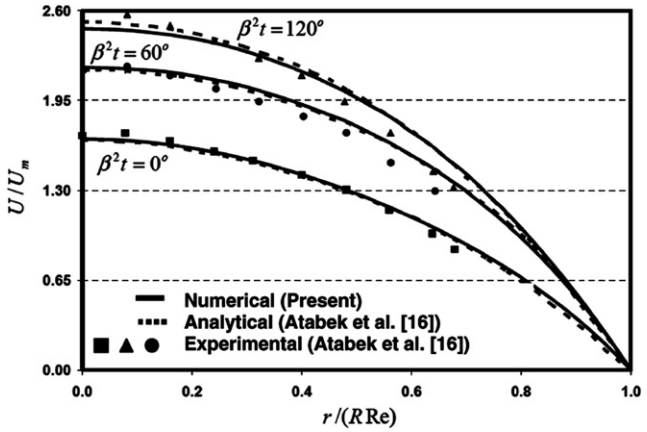

Fig. 3. Comparison of the axial velocity profiles between the present results and those of Atabek and Chang [16].

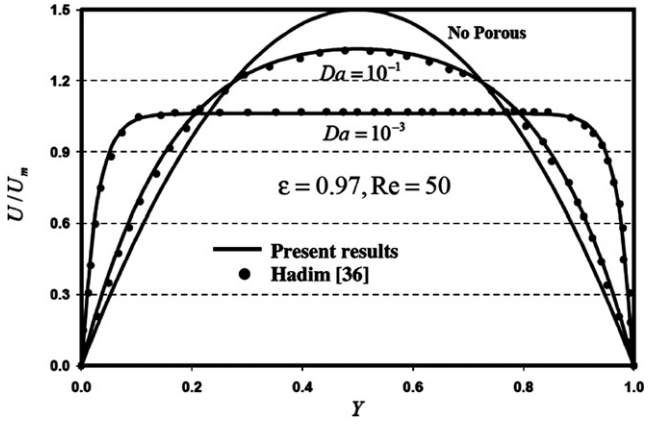

Fig. 4. Comparison of the fully developed velocity profile in the fully porous channel between the present work and that of Hadim [36] for various Darcy numbers ($Da = K/H^2$; K is the permeability of the porous medium and H is the height of the channel).

the inlet length of a pipe and both sets of data were in excellent agreement (Fig. 3). As an additional check on the accuracy of our work, we compared the fully developed velocity profile that we obtained in a fully porous channel with the results of Hadim [36] for various Darcy numbers as depicted in Fig. 4. Fig. 4 illustrates an excellent agreement between both results.

6. Results and discussion

The behavior of physiological flow through a rigid vessel is compared against a sinusoidal flow waveform, in the absence of an arterial wall, in terms of temperature and heat flux. The results of these comparisons are summarized in Figs. 5 and 6. Fig. 5 summarizes the results of the comparison of the radial temperature profiles along a plane passing through the middle of a tumor at three points corresponding to beginning of systole, peak systolic, and peak backward (end of systolic) flow conditions for both waveforms at Reynolds number of 300. This figure illustrates that the temperature profiles are flattened for more than 80% of the radius and they do not vary within a cycle for both waveforms. A steep variation in the temperature profiles for both waveforms is depicted in a narrow region close to the blood vessel wall due to the existence of a thin thermal boundary layer at the wall. Fig. 5 also shows that the sinusoidal waveform results in lower temperatures than the physiological waveform at different flow conditions. For instance, at the end of systole where both flows occur in reverse direction, the sinusoidal waveform results in lower temperature than the physiological waveform due to the fact that the magnitude of flow rate for the former waveform is larger than for the physiological waveform (see for instance Fig. 2). The results of variation with time of the normalized heat flux transferred to blood flow between both waveforms are depicted in Fig. 6. This figure illustrates a significant difference between both waveforms. As such, the sinusoidal waveform exhibits higher heat flux than the physiological waveform. This is associated with larger temperature gradients for sinusoidal than for physiological waveforms (see Fig. 5).

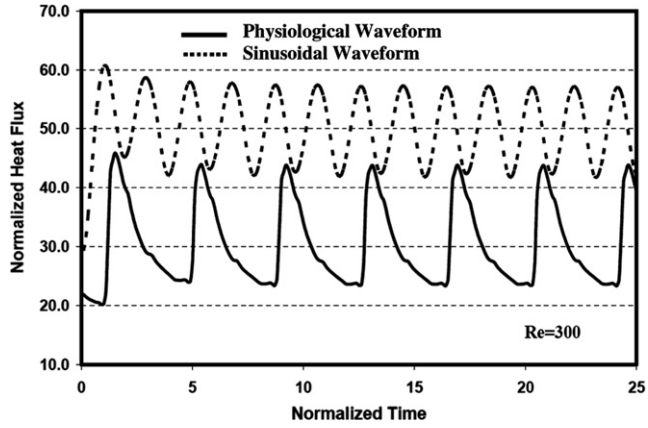

Fig. 6. Comparison of the normalized heat flux distribution between physiological and sinusoidal waveforms in the absence of an arterial wall.

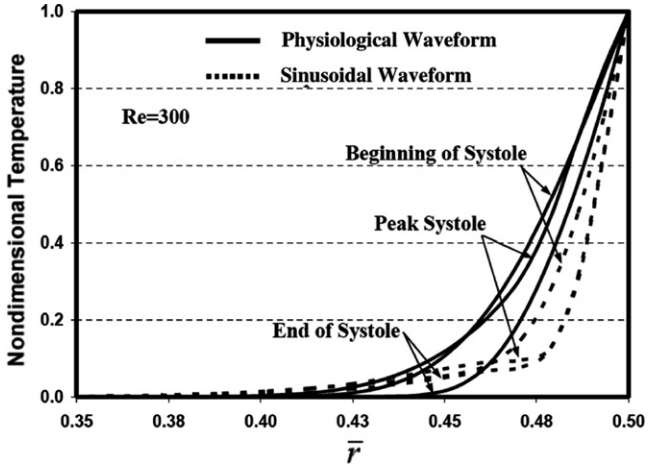

Fig. 5. Comparison of the normalized temperature distribution between physiological and sinusoidal waveforms in the absence of arterial wall $\left(\theta = \frac{T - T_{\text{inlet blood}}(37\ ^\circ\text{C})}{T_{\text{tumor}} - T_{\text{inlet blood}}(37\ ^\circ\text{C})}\right)$.

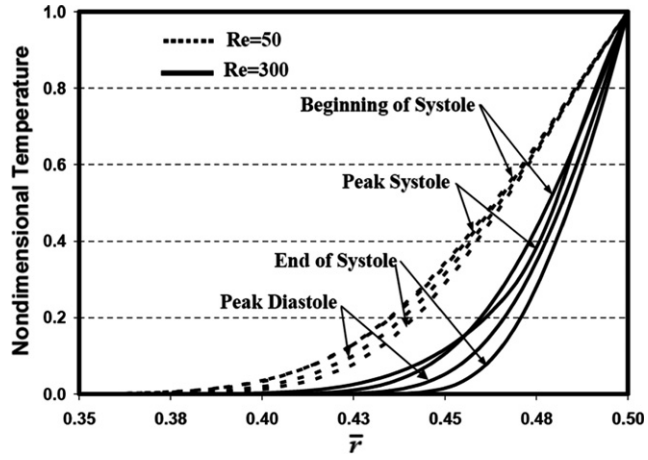

Fig. 7. Temporal variation of the temperature distribution for various flow conditions.

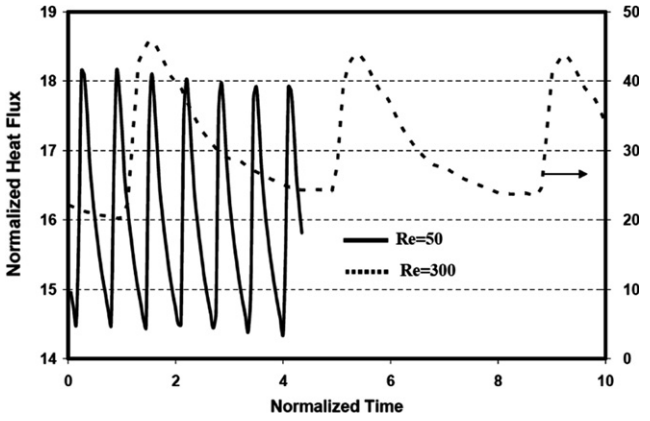

Fig. 8. Temporal variation of the normalized heat flux for different Reynolds numbers.

The effect of vessel size on the radial temperature profiles along a plane passing through the middle of the tumor for various flow conditions using a physiological waveform is shown in Fig. 7. Large vessels ($Re = 300$) exhibit large temperature gradients than smaller vessels ($Re = 50$). As such, the dissipation of heat from heated tissues, which is carried out by convection and conduction, is greater for large vessels (Fig. 8) due to a strong cooling effect. As a consequence, the cooling effect of the blood flow in large vessels results in under dosage of select tumor parts, which may contribute to the failure of arrest of tumor growth following hyperthermia treatment. This could be the consequence of a part of the surrounding tumor not reaching the desired treatment temperature.

The aforementioned results ignore the effect of the arterial wall on the temperature distribution. The influence of the arterial wall on the radial temperature profiles for different flow conditions using a physiological waveform (Fig. 9) highlights the importance of taking into consideration the presence of the arterial wall when modeling heat transfer during hyperthermia treatment. When an arterial wall exists between blood vessel and the surrounding tissue ($\bar{r} = 0.5$) the interface temperature is lower than without the arterial wall for various flow conditions (Fig. 9). Further, heat transfer through the surrounding tissue is mainly by conduction as depicted by a linear variation of temperature in the arterial wall.

We also studied the impact of different heating protocols on the transient temperature distribution in the blood vessel and the arterial wall. Fig. 10 compares the various heating schemes obtained with different waveforms. Uniform and pulsed heating schemes are used in this work. Uniform heating schemes exhibit higher temperature distributions than pulsed heating schemes at various flow conditions as depicted in Fig. 11. To achieve and maintain constant temperature during a uniform heating scheme, heating power needs to be on long enough to produce the desired rise in temperature. However, prolonged heating time may induce areas of overheating (beyond the therapeutic regions) that could damage normal tissues. Fig. 12 illustrates the effect of heating duration on the temperature distribution during a pulsed heating scheme at peak flow conditions. Higher temperature is depicted for longer periods of heating. When the heating power is turned off, the actual temperature of

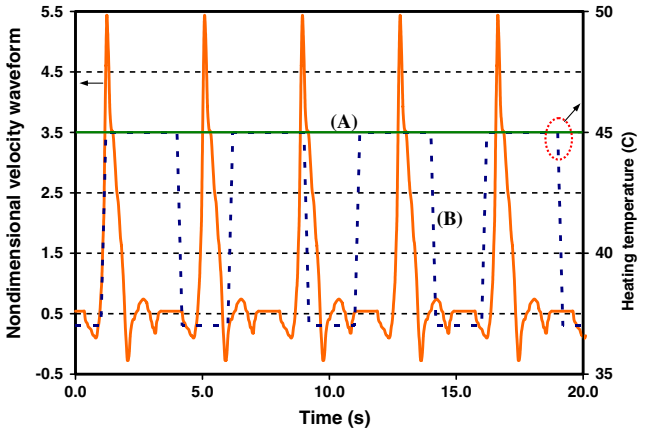

Fig. 10. Variation of different heating scheme: (A) uniform heating scheme and (B) pulsed heating scheme (interval: 3 s).

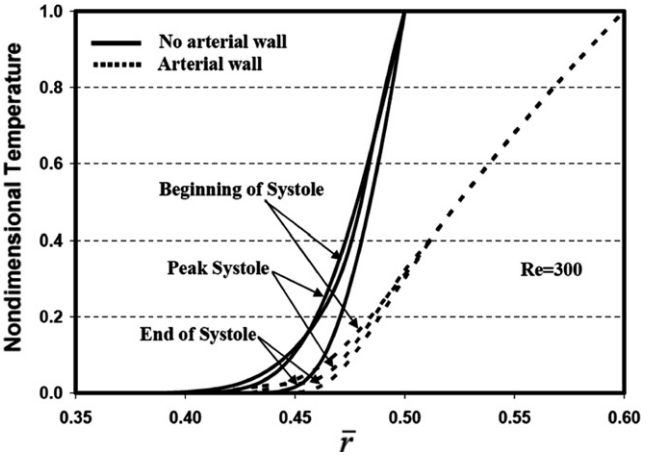

Fig. 9. Influence of arterial wall on temperature distribution for various flow conditions.

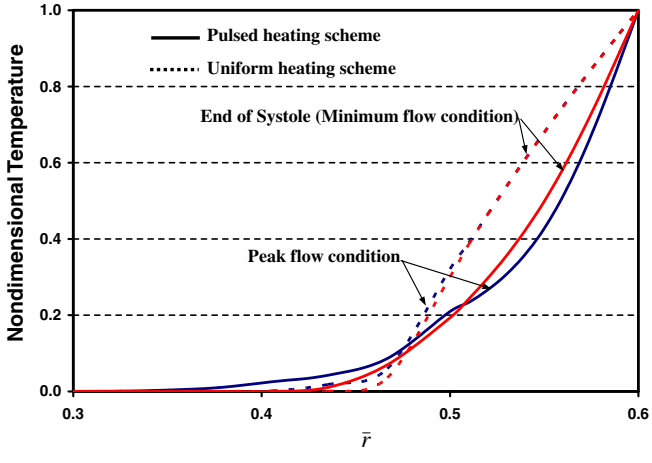

Fig. 11. Influence of the heating protocol on the temperature distribution at various flow conditions ($Re = 300$).

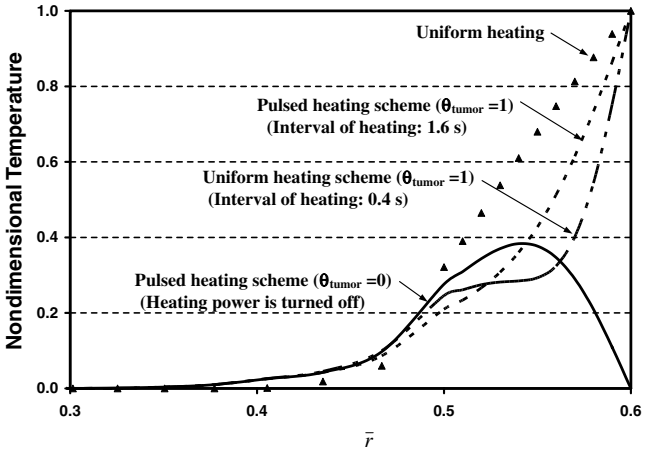

Fig. 12. Influence of the heating interval on the temperature distribution at peak flow condition ($Re = 300$) for pulsed heating scheme.

the heating target is decreased, however, a higher temperature is observed within the arterial wall due to the transient effect of heat.

7. Conclusions

A numerical study was conducted to determine the influence of pulsatile flow and the heating scheme on temperature distributions in blood vessel and tumor tissues using a physiological waveform at time-averaged Reynolds number of 50 and 300 and a sinusoidal flow waveform. The arterial wall was treated as macroscopically homogeneous porous media and modeled using the volume-averaged porous media equations. We showed that the presence of large vessels has a significant effect on temperature distributions and must be accounted for when planning hyperthermia treatment. Further, larger vessels are found to exhibit steeper temperature gradients than small vessels and consequently larger heat transfer rates. The presence of arterial wall is found to have a profound effect on the temperature distribution, heat transfer characteristics, and consequently on the hyperthermia treatment. Uniform heating scheme was found to exhibit larger temperature distribution than for pulsed heating scheme. Therefore, the domain of the thermal lesion may go beyond the therapeutic region to the normal tissue.

Acknowledgement

This work was supported by the Frankel Vascular Research Fund.

References

[1] J. Overgaard, D.G. Gonzales, M.C. Hulshof, G. Arcangeli, O. Dahl, O. Mella, S.M. Bentzen, Hyperthermia as an adjuvant to radiation therapy of recurrent or metastatic melanoma: a multicenter randomized trial by the European society for hyperthermic oncology, Int. J. Hyperther. 12 (1996) 3–20.

[2] J.R. Oleson, D.A. Sim, M.R. Manning, Analysis of prognostic variables in hyperthermia treatment of 161 patients, Int. J. Radiat. Oncol. Biol. Phys. 10 (1984) 2231–2239.

[3] M.W. Field, T.V. Dewhirst, Hyperthermia in the Treatment for Cancer, Upjohn, Kalamazoo, MI, 1988.

[4] S.B. Field, J.W. Hand, An Introduction to the Practical Aspects of Hyperthermia, Taylor & Francis, New York, 1990.

[5] J. Crezee, J.W. Lagendijk, Temperature uniformity during hyperthermia: the impact of large vessels, Phys. Med. Biol. 37 (1992) 1321–1337.

[6] C.M. Beacco, S.R. Mordon, J.M. Bruneaud, Development and experimental in vivo validation of mathematical modeling of laser coagulation, Laser Surg. Med. 14 (1994) 362–373.

[7] H.S. Reinhold, B. Endrich, Tumor microcirculation as a target for hyperthermia, Int. J. Hyperther. 2 (1986) 111–137.

[8] J.W. Baish, Formulation of a statistical model of heat transfer in perfused tissue, J. Biomech. Eng. 116 (1994) 521–527.

[9] D.E. Lemons, S. Chien, L.I. Crawshaw, S. Weinbaum, L.M. Jiji, Significance of vessel size and type in vascular heat transfer, Am. J. Physiol. 253 (1987) R128–R135.

[10] W. Levin, M.D. Shem, B. Cooper, R.E. Hill, J.W. Hunt, E.F. Liu, The effect of vascular occlusion on tumor temperatures during superficial hyperthermia, Int. J. Hyperther. 10 (1994) 495–505.

[11] R.B. Roemer, The local tissue cooling coefficient: a unified approach to thermal washout and steady-state perfusion calculations, Int. J. Hyperther. 6 (1990) 421–430.

[12] M.C. Kolios, M.D. Sherar, J.W. Hunt, Large blood vessel cooling in heated tissues: a numerical study, Phys. Med. Biol. 40 (1995) 477–494.

[13] M.C. Kolios, A.E. Worthington, D.W. Holdsworth, M.D. Sherar, J.W. Hunt, An investigation of the flow dependence of temperature gradients near large vessels during steady state and transient tissue heating, Phys. Med. Biol. 44 (1999) 1479–1497.

[14] J.R. Womersley, Oscillatory motion of a viscous liquid in a thin walled elastic tube. I: The linear approximation for long waves, Philos. Mag. 46 (1955) 199–221.

[15] S. Uchida, The pulsating viscous flow superimposed on the steady laminar motion of incompressible fluid in a circular pipe, Z. Angew. Math. Phys. 7 (1956) 403–422.

[16] H.B. Atabek, C.C. Chang, Oscillatory flow near the entry of a circular tube, Z. Angew. Math. Phys. 12 (1961) 185–201.

[17] H.B. Atabek, C.C. Chang, L.M. Fingerson, Measurement of laminar oscillatory flow in the inlet length of a circular tube, Phys. Med. Biol. 9 (1964) 219–227.

[18] R. Siegel, M. Perlmutter, Heat transfer for pulsating laminar duct flow, ASME J. Heat Transfer 8 (1962) 111–116.

[19] H.W. Cho, J.M. Hyun, Numerical solutions of pulsating flow and heat transfer characteristics in a pipe, Int. J. Heat Fluid Flow 11 (1990) 321–330.

[20] S.Y. Kim, B.H. Kang, J.M. Hyun, Heat transfer in the thermally developing region of a pulsating channel flow, Int. J. Heat Mass Transfer 36 (1993) 4257–4266.

[21] T.Z. Shih, H.L. Liu, A.T. Horng, Cooling effect of thermally significant blood vessels in perfused tumor tissue during thermal therapy, Int. Commun. Heat Mass Transfer 33 (2006) 135–141.

[22] O.I. Craciunescu, C.T. Clegg, Pulsatile blood flow effects on temperature distribution and heat transfer in rigid vessels, ASME J. Biomech. Eng. 123 (2001) 500–505.

[23] Z.J. Huang, J.M. Tarbell, Numerical simulation of mass transfer in porous media of blood vessel walls, Am. J. Physiol. 273 (1997) H464–H477.

[24] G. Karner, K. Perktold, H.P. Zehentner, Computational modeling of macromolecule transport in the arterial wall, Comput. Meth. Biomech. Biomed. 4 (2001) 491–504.

[25] K. Vafai, C.L. Tien, Boundary and inertia effects on flow and heat transfer in porous media, Int. J. Heat Mass Transfer 24 (1981) 195–203.

[26] K. Vafai, C.L. Tien, Boundary and inertia effects on convective mass transfer in porous media, Int. J. Heat Mass Transfer 25 (1982) 1183–1190.

[27] B. Alazmi, K. Vafai, Analysis of fluid flow and heat transfer interfacial conditions between a porous medium and a fluid layer, Int. J. Heat Mass Transfer 44 (2001) 1735–1749.
[28] K. Khanafer, K. Vafai, A. Kangarlu, Computational modeling of cerebral diffusion – application to stroke imaging, Magn. Reson. Imaging 21 (2003) 651–661.
[29] D.A. Nield, Modeling fluid flow in saturated porous media and at interfaces, in: D.B. Ingham, I. Pop (Eds.), Transport Phenomena in Porous Media II, Pergamon, Oxford, 2002, pp. 1–19.
[30] D.B. Ingham, I. Pop (Eds.), Transport Phenomena in Porous Media, vol. III, Elsevier, Oxford, 2005.
[31] I. Pop, D.B. Ingham, Convective Heat Transfer: Mathematical and Computational Modeling of Viscous Fluids and Porous Media, Pergamon, Oxford, 2001.
[32] C. Mills, I. Gabe, J. Gault, D. Mason, J. Ross, E. Braumwald, J. Shillingford, Pressure-flow relationships and vascular impedance in man, Cardiovasc. Res. 4 (1970) 405–417.
[33] E. Pedersen, A. Yoganathan, X. Lefebvre, Pulsatile flow visualization in a model of the human abdominal aorta and aortic bifurcation, J. Biomech. 25 (1992) 935–944.
[34] E. Pedersen, H. Sung, A. Burlson, A. Yoganathan, Two-dimensional velocity measurements in a pulsatile flow model of the normal abdominal aorta simulating different hemodynamic conditions, J. Biomech. 26 (1993) 1237–1247.
[35] M. Prosi, P. Zunino, K. Perktold, A. Quarteroni, Mathematical and numerical models for transfer of low-density lipoproteins through the arterial walls: a new methodology for the model set up with applications to the study of disturbed luminal flow, J. Biomech. 38 (2005) 903–917.
[36] H. Hadim, Forced convection in a porous channel with localized heat sources, ASME J. Heat Transfer 116 (1994) 465–470.